Photocatalytic production of hydrogen on Ni/NiO/$KNbO_3$/CdS nanocomposites using visible light†

Jina Choi,[a] Su Young Ryu,[a] William Balcerski,[a] T. K. Lee[b] and Michael R. Hoffmann*[a]

Received 4th December 2007, Accepted 12th March 2008
First published as an Advance Article on the web 2nd April 2008
DOI: 10.1039/b718535a

The photocatalytic production of H_2 from water splitting was demonstrated on Ni/NiO/$KNbO_3$/CdS nanocomposites using visible light irradiation at wavelengths >400 nm in the presence of isopropanol. The inherent photocatalytic activity of bulk-phase CdS was enhanced by combining Q-sized CdS with $KNbO_3$ and Ni deposited on $KNbO_3$. Enhanced activity is most likely due to effective charge separation of photogenerated electrons and holes in CdS that is achieved by electron injection into the conduction band of $KNbO_3$ and the reduced states of niobium (*e.g.*, Nb(IV) and Nb(III)) are shown to contribute to enhanced reactivity in the $KNbO_3$ composites by mediating effective electron transfer to bound protons. We also observed that the efficient attachment of Q-size CdS and the deposition of nickel on the $KNbO_3$ surface increases H_2 production rates. Other factors that influence the rate of H_2 production including the nature of the electron donors and the solution pH were also determined. The Ni/NiO/$KNbO_3$/CdS nanocomposite system appears to be a promising candidate for possible practical applications including the production of H_2 under visible light.

Introduction

Hydrogen (H_2) production from water splitting using semiconductor photocatalysts has attracted considerable interest since the pioneering work of Fujishima and Honda,[1] who discovered that water can be photo-electrochemically decomposed into hydrogen and oxygen using a semiconductor (TiO_2) electrode under UV irradiation. A large number of metal oxides and sulfides (*e.g.* TiO_2,[1–3] WO_3,[4–6] $SrTiO_3$,[7,8] ZnO,[9–11] CdS,[12–17] ZnS,[13,16,18,19] niobates,[20–24] and tantalates[25–28]) have been examined as photocatalysts for hydrogen production from splitting water. However, the majority of the simple and mixed-metal oxides photocatalysts are primarily active for H_2 production under UV irradiation ($\lambda < 385$ nm or $E_g \geq 3.0$ eV) present in only a small portion of solar light. More recently, there is a focused effort on the development of photocatalysts that are capable of using visible light ($\lambda = 400$–700 nm) for the photocatalytic production of H_2 including transition metal doping (*e.g.*, platinum,[29] chromium,[30] and vanadium[31]) and nonmetallic element doping (*e.g.*, nitrogen,[32–35] sulfur,[36,37] and carbon[35,38]).

CdS, n-type semiconductor with $E_g = 2.4$ eV, has been shown to have photocatalytic activity for H_2 production under visible light irradiation, although, sacrificial electron donors such as C_2H_5OH,[39] HS^-,[40,41] or SO_3^{2-} [19] are used to obtain measurable rates of H_2 production and to avoid the photocorrosion of CdS in the presence of O_2. On the other hand, the electronic levels and photoactivity of CdS can be tuned by changing or controlling particle size without changing the chemical composition. For example in the case of nanoparticulate ZnO, Hoffmann and co-workers[9,42] reported a ten-fold increase in photoefficiency for the photocatalytic production of hydrogen peroxide with a decrease in particle size from 40 to 23 nm. In another example, Hoffman *et al.*[43] found an increase in quantum efficiency for photo-polymerization of methyl methacrylate with a corresponding decrease in particle size using Q-size CdS.

In order to enhance the photocatalytic activity of CdS, efforts have been made to combine CdS with other semiconductors having different band energies (*e.g.*, TiO_2,[44–47] ZnS,[13,48,49] $K_4Nb_6O_{17}$,[50] or $K_2Ti_4O_9$[51,52]) since the coupling of two semiconductor particles with different energy levels is useful to achieve effective charge separation. For example in a colloidal TiO_2/CdS composite system, the electrons photogenerated from CdS band gap excitation can be transferred to the conduction band (CB) of TiO_2 particles, while the holes remain in the CdS particle. It is also observed that this charge separation in a colloidal composite system can accelerate the degradation of azo dyes[44] and increase H_2 production in aqueous H_2S solution.[46]

In this study, we synthesized nanocomposites of potassium niobate ($KNbO_3$) and CdS by solid-state reactions and investigated their properties and photoactivity for H_2 production under visible light irradiation ($\lambda > 400$ nm) in the presence of isopropanol as an electron donor. $KNbO_3$ is used in optical waveguides, in nonlinear optical devices (*e.g.*, frequency doubling and wavelength mixing), in piezoelectric devices (*e.g.*, tunable frequency ultrasound transducers), in holographic image storage, and as a wide-band gap photocatalyst ($\Delta E_g = 3.4$ eV) because of its unusual chemical and physical properties. $KNbO_3$/CdS nanocomposites are characterized by XRD, SEM, TEM, UV-vis reflectance spectra and show better visible-light photoactivity for H_2 production than other composites (*e.g.*, TiO_2 or $K_4Nb_6O_{17}$). Moreover, the efficiency of H_2 production is significantly enhanced by loading Ni on $KNbO_3$.

[a]*W. M. Keck Laboratories, California Institute of Technology, Pasadena, California, 91125, USA. E-mail: mrh@caltech.edu; Tel: +1 626 395 4391*
[b]*Nanopac, 878-6 Hanyang Plaza 5th Floor, Youngtong-dong, Youngtong-ku, Suwon, 443-812, Korea. E-mail: tklee@nano-pac.com; Tel: +82 31 203-6697*

† This paper is part of a *Journal of Materials Chemistry* theme issue on hydrogen storage and generation. Guest editor: John Irvine.

Experimental

Sample preparation

Stoichiometric $KNbO_3$ was synthesized from Nb_2O_5 (Aldrich) and K_2CO_3 (Aldrich) in a standard solid-state reaction. K_2CO_3 and Nb_2O_5 were mixed together in a mortar at 1 : 1 mole ratio and the powdered mixture was pressed into a pellet at 27.6 MPa and then heated at 650–925 °C for 10 h with a heating and cooling temperature ramp of ±200 °C h^{-1}. With slight variations of the K : Nb mole ratio of 1 : 1.1 and a heating temperature at 1025 °C, a mixture of $KNbO_3$ and $K_4Nb_6O_{17}$ is obtained. Synthesis of $K_4Nb_6O_{17}$ was carried out for comparison using K_2CO_3 and Nb_2O_5 in the K : Nb mole ratio of 1 : 1.5 and calcination at 1150 °C for 10 h. The crystal structures were confirmed by X-ray diffraction (XRD) at room temperature.

$KNbO_3$/CdS composite samples were prepared by stirring $KNbO_3$ powders in a 20 mL of ethanol of 2×10^{-2} M $Cd(CH_3COO)_2 \cdot 2H_2O$ for 1 day, followed by sulfurization with 20 mL of ethanol of 2×10^{-2} M Na_2S for 1 day. Composite samples were collected by filtration, which was followed by washing and subsequent drying.

Elemental nickel (Ni) and NiO (0.1–3.6 wt%) were loaded on the surface of $KNbO_3$ by a method that Domen and co-workers[23,53,54] reported. $KNbO_3$ samples were suspended in a $Ni(NO_3)_2$ aqueous solution for 1 day, followed by it being filtered, washed and dried. The solid was reduced in H_2 atmosphere at 500 °C for 2 h, and subsequently oxidized in an O_2 atmosphere at 200 °C for 1 h. In the case of elemental Ni-loaded $KNbO_3$ samples ($Ni/KNbO_3$), the O_2 oxidation step was eliminated. The NiO-loaded $KNbO_3$ samples ($NiO/KNbO_3$) were obtained by complete O_2 oxidation at 500 °C for 1 h. A schematic flow chart is shown in Fig. 1.

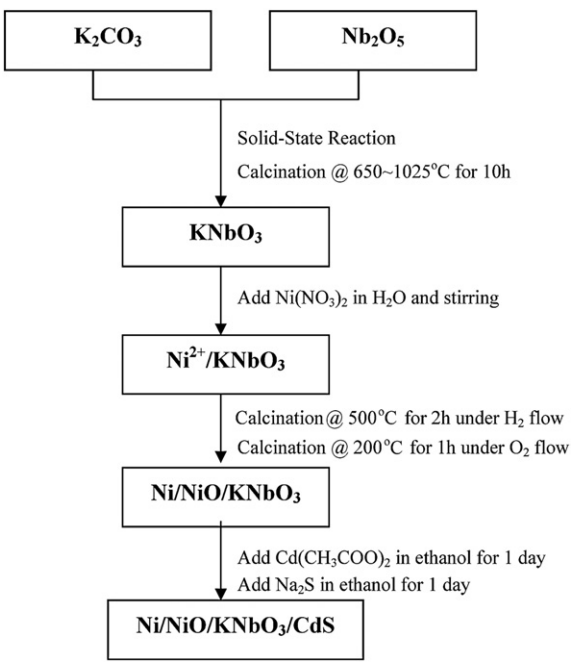

Fig. 1 Schematic flow chart outlining the synthetic procedures for the composite $Ni/NiO/KNbO_3/CdS$ catalyst preparation.

Characterization

The crystal structures of synthesized $KNbO_3$ samples were confirmed by powder X-ray diffraction (XRD) using a Philips diffractometer (X'pert Pro) with Cu-Kα radiation. Diffuse reflectance spectra were obtained with a UV-vis spectrometer (Shimadzu UV-2101 PC) and were converted from reflection to absorption spectra by the Kubelka–Munk method. Brunauer–Emmett–Teller (BET) surface area analyses were also performed to compare the surface areas of $KNbO_3$ samples that were prepared under different conditions. Microstructures and composition were also analyzed with a LEO 1550 VP Field Emission Scanning Electron Microscope (SEM) and a Philips EM201 Transmission Electron Microscope (TEM). Inductively Coupled Plasma-Mass Spectrometry (HP 4500 ICP-MS) was used to determine the amounts of Ni^{2+} and Cd^{2+} adsorbed on the surface of $KNbO_3$. Potassium ions released from $KNbO_3$ during ion exchange with Ni^{2+} were determined by a Dionex DX-500 Ion Chromatography system. X-Ray Photoelectron Spectroscopy (XPS) was used to observe the changes in the oxidation state of Nb species and Ni species adsorbed on the surface of $KNbO_3$ with Al-Kα radiation.

Photocatalytic reaction

Photocatalytic reactions for hydrogen production were carried out in an air-tight reactor vessel under visible light irradiation ($\lambda > 400$ nm). Catalyst samples (0.2 g) were suspended in 50 mL of a water–isopropanol mixture (30 v/v%) in a Pyrex glass reactor. Samples were purged with Ar or N_2 gas for 30 min before reaction in order to eliminate dissolved O_2. A high-pressure 500 W Hg–Xe arc lamp in combination with a 400 nm cut-off filter was used as the primary light source. The intensity of incident light was determined by ferrioxalate actinometry to obtain quantum yields for H_2 production. The amount of H_2 evolved during photolysis was analyzed by GC/TCD (HP 5890, N_2 carrier) with a molecular sieve column (30 m × 0.32 mm × 12.00 μm).

Results and discussion

$Ni/NiO/KNbO_3/CdS$ nanocomposite characterization

Fig. 2 shows XRD patterns of synthesized $KNbO_3$ under different calcination temperatures and mole ratios. XRD pattern for $KNbO_3$ calcined at 925 °C with 1 : 1 mole ratio of K : Nb (Fig. 2(a)) shows exactly the same 2θ peaks that correspond to standard $KNbO_3$. Samples calcined over the range of temperatures from 650 to 925 °C also show the same peak patterns. However, the sample produced at 1025 °C with 1 : 1.1 mole ratio of K : Nb (Fig. 2(b)) has extra 2θ peaks that are attributed to potassium hexaniobate ($K_4Nb_6O_{17}$). $K_4Nb_6O_{17}$ has a perovskite structure similar to $KNbO_3$, but it consists of a layered structure composed of two different types of niobate sheets. The material structures were also confirmed by SEM images. A layered structure is only observed for the sample calcined at 1025 °C by SEM as shown in Fig. 3. The diffraction peaks of $KNbO_3$ samples are more intense and sharper with an increase in calcination temperature. The broadening of XRD peaks at low calcination temperatures may be due to smaller crystallite sizes.

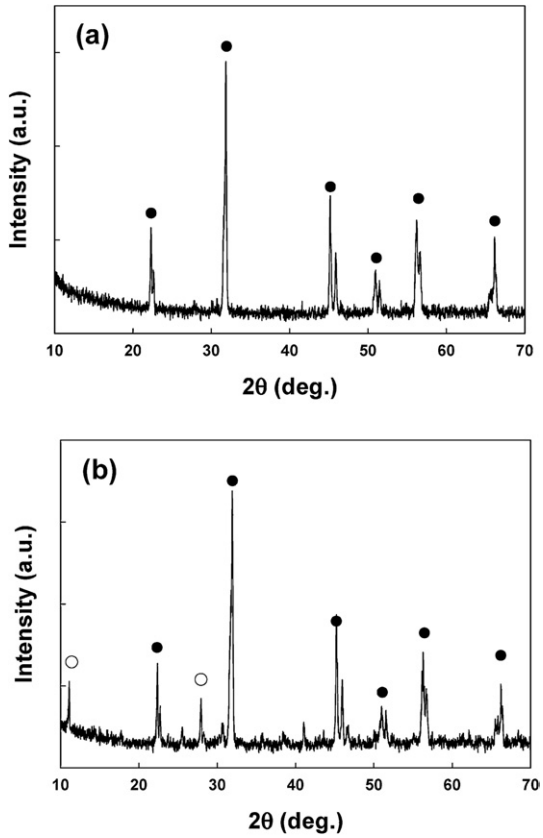

Fig. 2 X-Ray diffraction patterns for (a) $KNbO_3$ powder sample synthesized from 1 : 1 mole ratio of K_2CO_3 and Nb_2O_5 at 925 °C and (b) $KNbO_3$ powder sample synthesized from 1 : 1.1 mole ratio of K_2CO_3 and Nb_2O_5 at 1025 °C. (●) $KNbO_3$, (○) $K_4Nb_6O_{17}$.

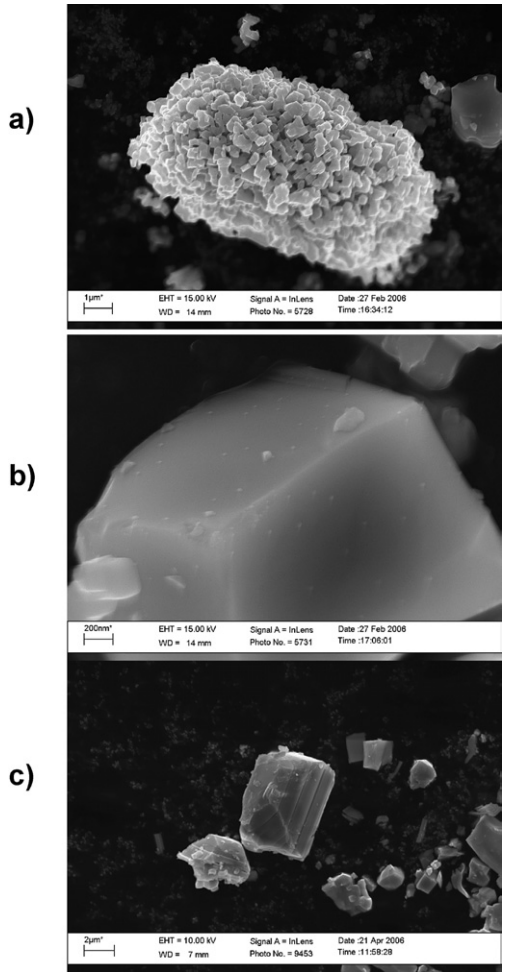

Fig. 3 SEM images of (a), (b) $KNbO_3$ synthesized at 925 °C (K : Nb = 1 : 1) and (c) $KNbO_3$ synthesized at 1025 °C (K : Nb = 1 : 1.1).

The particle sizes of $KNbO_3$ at different calcination temperatures can be estimated with the Scherrer equation; the estimated particle sizes were 28, 32 and 39 nm for $KNbO_3$ samples prepared at 650 °C, 775 °C and 925 °C, respectively. BET surface areas were found to be 4.35, 3.08 and 2.14 $m^2\ g^{-1}$ for 650 °C, 775 °C and 925 °C samples, respectively, and it is apparent that the specific surface area decreases with an increase in calcination temperature. Furthermore, there appears to be no observable structural difference between $KNbO_3$ samples before and after Ni deposition or with the addition of nanoparticulate CdS. Fig. 4 is the TEM picture of a nanocomposite sample of Ni/NiO/$KNbO_3$/CdS which shows that Ni or CdS nanoparticles were loaded on the surface of $KNbO_3$.

Fig. 5 shows the light absorption properties of nanocomposite samples. The $KNbO_3$/CdS nanocomposite absorbs visible light at $\lambda > 400$ nm. This is primarily due to the band gap excitation of Q-size CdS, since $KNbO_3$ does not absorb visible light. The respective band gaps are estimated to be 3.4 eV and 2.6 eV for $KNbO_3$ and Q-CdS, from the plots of Kubelka–Munk functions *vs.* photon energy. It should be noted that absorption edge of Q-size CdS synthesized for the CdS/$KNbO_3$ nanocomposite is blue-shifted from absorption edge of bulk CdS particles.[43]

The synthesized $KNbO_3$ samples were suspended in an aqueous $Ni(NO_3)_2$ solution for 1 day to load Ni^{2+} as a co-catalyst. ICP-MS and IC results show that most of the Ni^{2+} ions are adsorbed on the surface of $KNbO_3$ particles and some of them

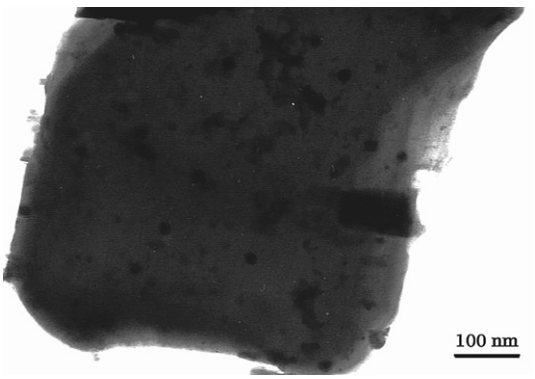

Fig. 4 TEM image of Ni/NiO/$KNbO_3$/CdS nanocomposite.

are ion-exchanged with K^+ ions located in the $KNbO_3$ framework. However, in the synthesis of CdS nanoparticles on the $KNbO_3$ surface, only 20–30% of Cd^{2+} ions are adsorbed on the surface and ion exchange with K^+ is not observed. Then Ni^{2+}-adsorbed (or ion-exchanged) $KNbO_3$ samples were treated under proper conditions, *i.e.* H_2 reduction at 500 °C followed by O_2 oxidation at 200 °C. After thermal reduction by H_2, the doped samples turned gray from the initial white undoped $KNbO_3$.

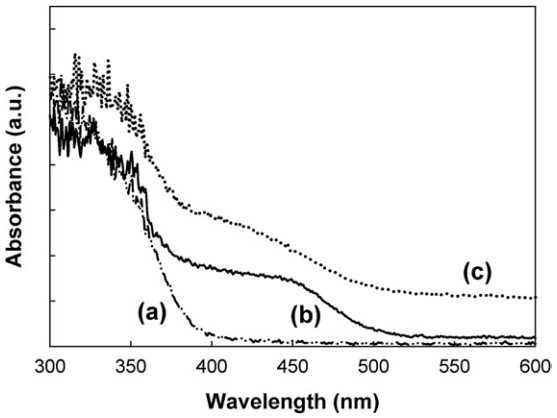

Fig. 5 UV-vis diffuse reflectance spectra for (a) $KNbO_3$, (b) $KNbO_3$/CdS, (c) Ni/NiO/$KNbO_3$/CdS.

However, oxidation at 500 °C converts elemental nickel to NiO with a corresponding change in color from gray to light yellow. XPS analysis of the various samples was used to identify the oxidation states of Ni in each sample.

Photocatalytic H_2 production

The measured H_2 production rates in illuminated aqueous isopropanol solutions under visible light with CdS, $KNbO_3$, Ni/NiO/$KNbO_3$, and Ni/NiO/$KNbO_3$/CdS composites are compiled in Table 1. The naked $KNbO_3$, nickel-doped $KNbO_3$, and Ni/NiO/$KNbO_3$, samples showed no activity for H_2 production under visible light since its band gap energy (3.4 eV) was larger than the excitation energies (λ > 400 nm). Simple Q-CdS nanoparticle suspensions produce H_2, but at very low rates. However, H_2 production rates increase significantly in the $KNbO_3$/CdS nanocomposites. This may be because effective charge separation of electrons and holes in illuminated CdS with electron injection into the conduction band of $KNbO_3$ may be possible in the $KNbO_3$/CdS nanocomposites. H_2 production with TiO_2 (Degussa P-25)/CdS nanocomposites was also performed for comparison. TiO_2/CdS had lower H_2 production activity than $KNbO_3$/CdS. H_2 production rates for the $KNbO_3$/CdS nanocomposites were enhanced significantly in the presence of the deposited Ni/NiO co-catalysts. Ni most likely serves to collect conduction band electrons. However, a significant enhancement of H_2 production rate was not observed in a Pt deposited $KNbO_3$ sample (Pt/$KNbO_3$/CdS) as compared to Ni/$KNbO_3$/CdS nanocomposites. We also synthesized potassium hexaniobate ($K_4Nb_6O_{17}$) for comparison because $K_4Nb_6O_{17}$ is known as a good photocatalyst for H_2 production under UV light irradiation.[20,22,23] However, the result shows that $KNbO_3$/CdS nanocomposite produces more H_2 than $K_4Nb_6O_{17}$/CdS under visible light irradiation.

Table 1 Photocatalytic activities of potassium niobate nanocomposites for H_2 production from water–isopropanol mixed solution

Sample	Weight% of Ni_T	Calcination temp./°C	H_2 production[a]/ μmol h^{-1} g^{-1}
$KNbO_3$	0	925	0
Ni/NiO/$KNbO_3$	0.1	925	0
CdS	0	—	3
TiO_2/CdS	0	—	12
Ni/NiO/$K_4Nb_6O_{17}$/CdS	0.1	1150	37
Ni/NiO/$KNbO_3$/CdS	0	925	50
	0.1	925	150
	0.3	925	125
	0.5	925	75
	1.0	925	80
	3.6	925	65
	0.5	650	110
	0.5	775	80
	1.0	650	120
	1.0	775	80

[a] Catalyst, 0.2 g; volume, 50 ml; light source, Hg–Xe lamp (500 W) with λ > 400 nm, 30 v/v% isopropanol.

The enhanced reactivity of the $KNbO_3$ nanocomposites may be due to involvement of the reduced states of niobium and/or oxygen vacancies that allow for the photoexcitation of mobile electrons with visible light. For example, Ewart *et al.*[55] reported that mobile electrons are generated in electrochemically reduced and Fe-doped $KNbO_3$ upon excitation at 532 nm. The electrons photoexcited at 532 nm had lifetimes of 4 ns and electron mobilities of 0.5 cm^2 V^{-1} s^{-1}. They concluded that the photoexcited electrons are trapped within 4 ns (*i.e.*, loss of detectable mobility), however, the trapped-state electrons are thermally activated on a millisecond timeframe and eventually recombine with the internal donor states. Kesselman *et al.*[56] observed a similar reduction in Nb_2O_5/TiO_2 composites that were reduced over hydrogen at high temperatures. Reduction of Nb_2O_5 is known to form a variety of phases such as $Nb_{12}O_{29}$, $Nb_{22}O_{54}$, $Nb_{25}O_{62}$, and $Nb_{47}O_{116}$ that involve partial oxygen loss coupled with the formation of Nb(IV). Therefore, the longer lifetimes (τ_{tr} > ms) of the trapped electrons may contribute to the higher reduction rates for bound protons or hydroxides. Similar mixed valence state phase should coexist within the framework of reduced $KNbO_3$ and contribute to the photo-excitation of electrons and to the overall photoactivity with visible light. The Ni/NiO/$KNbO_3$ samples were thermally treated at 500 °C under H_2 atmosphere to reduce Ni^{2+} to elemental nickel. This treatment step may lead to creation of oxygen vacancies or formation of the reduced states (*e.g.*, Nb(IV) and Nb(III) states) of niobium. The thermal treatment of pure, white $KNbO_3$ at 500 °C under H_2 produced a light gray product that is consistent with Nb(V) reduction. We performed XPS analysis to compare the oxidation states of Nb between $KNbO_3$ samples before and after H_2 reduction, however, the reduced states were not readily observed. However, it was measured that reduced states of Nb are formed during the photolytic reaction. Another relevant feature of the metal niobates (*e.g.*, $LiNbO_3$[57] and $KNbO_3$[58]), which is critical for electro-optic and photorefractive applications, is the activation of surface protons (*i.e.*, protons bound in hydroxyl ions, $^-$OH). The hydroxyl bound protons have activation energies in the range of 1 eV for mobility in $KNbO_3$ crystals.

In light of the above photophysical properties related to surface hydroxyl groups, an alternative pathway may involve excitation of reduced $KNbO_3$ with visible light followed by conduction band reduction of surface bound protons on $KNbO_3$. The pH of zero point of charge, pH_{zpc}, of $KNbO_3$ was measured as pH ~ 3.2, thus the $KNbO_3$ surface may be dominated by

>NbOH and >NbO$^-$ under our optimal experimental conditions (pH $\sim$ 8). Given this situation, we can write the following set of reactions that may result in H_2 production on $KNbO_3$ surface sites or Ni/NiO/$KNbO_3$ composite sites:

$$KNb^{V}O_3 \xrightarrow[H_2]{T=500\ ^\circ C} KNb^{IV}O_3 \quad (1)$$

$$KNb^{IV}O_3 + h\nu \xrightarrow{530nm} e^-_{cb} + h^+_{vb} \quad (2)$$

$$>Nb^{IV}ONb^{IV}< + H_2O \rightleftarrows 2>Nb^{IV}OH \quad (3)$$

$$>Nb^{IV}OH \overset{K^s_{a2}}{\rightleftharpoons} >Nb^{IV}O^- + H^+ \quad (4)$$

$$> Nb^{IV}OH + e^-_{cb} \rightarrow >Nb^{IV}O^- + H^\bullet \quad (5)$$

$$2H^\bullet \rightarrow H_2 \quad (6)$$

In addition, we compared three different procedures for attachment of CdS particles on the $KNbO_3$ surface as shown in Fig. 6. To form $KNbO_3$/CdS nanocomposites, we first added Cd^{2+} ions in $KNbO_3$ suspension, and then we added sulfide (HS^-/S^{2-}) ions after stirring for 1 day (Fig. 6(a)). ICP-MS results show that only 20–30% of the Cd in CdS particles are directly synthesized on $KNbO_3$ surface and the remainder of the CdS particles are suspended freely in the solution. One sample was prepared by mechanical mixing of CdS and $KNbO_3$ by addition of $KNbO_3$ after Q-CdS synthesis in ethanol (Fig. 6(b)) and another sample has only CdS adsorbed on the $KNbO_3$ surface by removing free Cd^{2+} ions in suspension before adding S^{2-} ions (Fig. 6(c)). The CdS surface adsorption sample (Fig. 6(c)) shows reasonable photoactivity even though the amounts of CdS are quite small (20–30%) compared to samples having CdS synthesized both on $KNbO_3$ surface and in solution (Fig. 6(a)). As a consequence, we conclude that direct CdS contact with the $KNbO_3$ surface plays an important role for effective charge separation with increased H_2 production rates. Although, the externally mixed sample (Fig. 6(b)) also has measurable H_2 production rates. From these results, we can infer that Q-CdS particles are attached to the surface of $KNbO_3$ under our experimental conditions (pH $\sim$ 8) even though CdS was synthesized initially in solution phase.

The $KNbO_3$ surface is negatively charged under the pH conditions of our experiments since the pH_{zpc} of $KNbO_3$ is measured as pH $\sim$ 3.2. The actual determination of pH_{zpc} of the nanoparticulate CdS colloids is more difficult. Park and Huang[59] reported a $pH_{zpc} = 7.5$ for colloidal CdS based on electrophoretic mobility measurements and acid–base titrations. At an ionic strength of $\mu = 0.05$ M, they determined that $pK^s_{a1} = 6.1$ and $pK^s_{a2} = 9.0$ for $[Cd^{2+}] = 2.5$ μM and $\sigma_0 = 20$ mC cm^{-2}. Liu and Huang[60] subsequently reported a pH_{zpc} for cubic CdS of 7.0 and $pH_{zpc} = 7.5$ for hexagonal CdS. In contrast, other researchers[61–63] have reported substantially lower values for the pH_{zpc} for CdS in aqueous suspensions. Under experimental conditions that were quite different from those employed by Park and Huang,[59] Nicolau and Menard[63] determined a $pH_{zpc} = 1.8$ for 0.01 M Na_2SO_4 and KCl as background electrolytes based on electrophoretic mobility measurements. Guindo *et al.*[62] found even lower values of pH_{zpc} between 1 and 1.5 for differently prepared spherical CdS particles. However, they pointed out that the IEP (isoelectric point) was sensitive to the specific surface characteristics of CdS which depend on the degree of oxidation or aging as noted by the shift in IEP to higher values for samples that were synthesized over longer periods of time. According to our observations, it may be true that pH_{zpc} of CdS is relatively high under our experimental conditions, so that CdS colloid in solution are positively charged and then electrostatically attracted to the negatively charged $KNbO_3$ particles under our experimental pH conditions.

The rates of H_2 production on the four-component composite, Ni/NiO/$KNbO_3$/CdS, are compared to the three-component composite containing only Ni or NiO. The data presented in Fig. 7 show that elemental Ni on $KNbO_3$ is a more active species than NiO on $KNbO_3$ to improve H_2 production although its external surface is partially oxidized to NiO. However, the H_2 production rates are not greatly enhanced in the three-component composite containing only NiO. This tendency is consistent

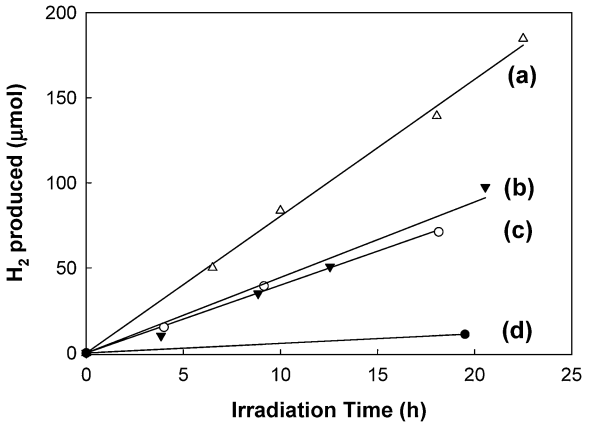

Fig. 6 Effect of CdS loading on $KNbO_3$ surface on photocatalytic activities for H_2 production: (a) CdS synthesized both on $KNbO_3$ surface and in solution, (b) CdS synthesized by external mixing with $KNbO_3$, (c) CdS adsorbed on $KNbO_3$, (d) Q-size CdS only.

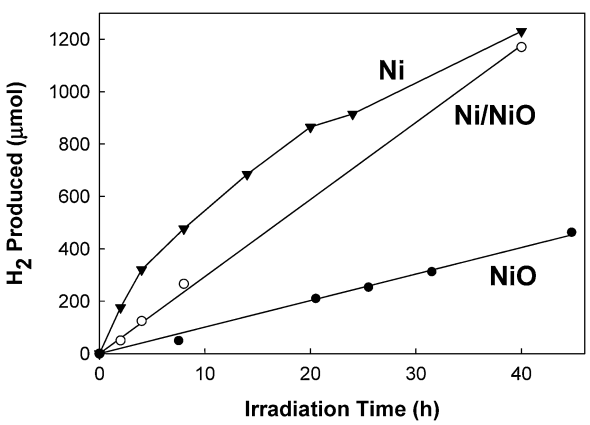

Fig. 7 Effect of oxidation states of Ni deposited $KNbO_3$ (0.1 wt% loading as Ni_T) on photocatalytic H_2 production from water–isopropanol mixed solution.

with previous results obtained for Ni/NiO loaded onto $SrTiO_3$ as reported by Domen *et al.*[53] They reported that Ni/NiO/$SrTiO_3$ produced substantially more H_2 from aqueous methanol than the simpler NiO/$SrTiO_3$ system under UV irradiation. They concluded that the presence of Ni metal in contact with the $SrTiO_3$ surface plays an important role in the H_2 production activity. Domen *et al.*[64] also found small amounts of H_2 evolved under the band gap irradiation of Ni/$SrTiO_3$. They attributed their low activity to loss of Ni by release of Ni^{2+} due to oxidation of Ni metal by direct hole transfer from $SrTiO_3$ during band gap irradiation. In contrast, our results show that the three-component, Ni/$KNbO_3$/CdS, composite can produce a comparable amount of H_2 compared to the four-component, Ni/NiO/$KNbO_3$/CdS, composite. In both the 3- and 4-component catalysts, the primary absorption occurs at $\lambda > 400$ nm (compared to $SrTiO_3$ with $\lambda < 400$ nm) with CdS as a chromophore. Thus, elemental nickel deposited on $KNbO_3$ is unlikely to be directly oxidized by holes in our composite material.

As shown in Table 1, the highest H_2 production rates were obtained with a Ni-deposition level of 0.1 wt% as Ni_T (= Ni + NiO), and above this level enhancement due to nickel deposition was marginal. However, we observed the enhanced H_2 production with higher wt% of Ni deposition on $KNbO_3$ samples prepared at low calcination temperatures. The increase of photoactivities with 0.5–1.0 wt% Ni-loaded on $KNbO_3$ prepared at low calcination temperatures may be only due to simply an increase in the total reactive surface area. It is noted that a $KNbO_3$ sample mixed with the $K_4Nb_6O_{17}$ structure which was calcined at 1025 °C produces comparable amounts of H_2 to $KNbO_3$ samples calcined at 925 °C.

We observed fairly dramatic color changes taking place during irradiation of the Q-size CdS and the CdS nanocomposite materials. In all cases, the catalysts suspensions are yellow before illumination because of the CdS chromophore. However, after exposure to a focused beam of light at $\lambda > 400$ nm, the color changes very quickly to a silver gray. As the color changes from yellow to gray, H_2 production is observed as a steady stream of gas bubbles rising up in the photolysis cell. The observed color change may be due to the rapid photoreduction of Cd(II) to Cd(I) and then to Cd(0) on the surface of CdS in the absence of oxygen. There is also some probability that S^{2-} in the CdS matrix is also oxidized partially by trapped valence band holes to form S(0) and eventually polysulfide ion (S_2^{2-}). Upon exposure to oxygen, the yellow color is regenerated over several hours with the return of yellow CdS on the nanocomposite structures.

Apparent quantum yields, ϕ, for H_2 production, were determined as follows:

$$\phi = \frac{\mathrm{d}m_{H_2}/\mathrm{d}t}{I^0_{abs}} \times 2 \quad (7)$$

where $\mathrm{d}m_{H_2}/\mathrm{d}t$ is the initial production rate of H_2 (mol s^{-1}) and I^0_{abs} is the photon absorption rate in units of Einstein s^{-1} (mol(e^-) s^{-1}). We also considered the fact that two electrons are consumed to produce one hydrogen molecule from two protons for quantum yield calculation. The photon flux through the cell was 2.3×10^{17} photons s^{-1} as determined by ferrioxalate actinometry with an apparent quantum yield for H_2 production of 4.4% for $\lambda > 400$ nm. It should be noted that the amount of light scattered from the nanocomposite suspension was not considered here and therefore the actual quantum yield may be higher.

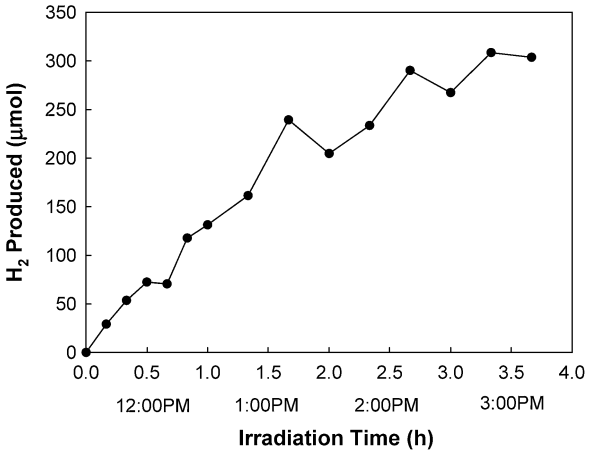

Fig. 8 H_2 production rate from water–isopropanol mixed solution with Ni/NiO/$KNbO_3$/CdS under natural sunlight (August 13, 2006; Pasadena, California).

Photocatalytic H_2 production under natural sunlight

Substantial amounts of hydrogen gas are also produced readily using natural sunlight as the irradiation source. For example, the 4-component composite was exposed to solar light between 11:30 am and 3:30 pm on the roof of W. M. Keck Laboratories at Caltech on August 13, 2006. Experimental procedures were identical to those employed in the controlled laboratory experiments except the use of different types of pyrex reactors. As shown in Fig. 8, H_2 is readily produced from aqueous isopropanol solutions under natural sunlight; however, the amount of H_2 produced is actually larger than that produced over the same period of time under UV light irradiation in the laboratory. This simple demonstration illustrates the potential of practical application of Ni/NiO/$KNbO_3$/CdS nanocomposite for H_2 production with sunlight.

Influence of solvent composition on photocatalytic H_2 production

The relative effects of a variation of solvent–water mixtures on H_2 production for $KNbO_3$/CdS at $\lambda > 400$ nm are illustrated as shown in Fig. 9. 30 v/v% of isopropanol (IPA), ethanol (EtOH), and methanol (MeOH) solution were used in the photoreaction. The order of photoreactivity is IPA > EtOH > MeOH, which is in inverse order of their dielectric constants (*i.e.*, $\varepsilon_{IPA} = 19 < \varepsilon_{EtOH} = 24.3 < \varepsilon_{MeOH} = 33$).

Alcohols function primarily as hole traps that prevent rapid electron–hole recombination. The presence of an electron donor other than water is crucial for photocatalytic H_2 production, since little H_2 is produced without added electron donors even under UV light irradiation. However, the interaction of the various electron donors with the charged CdS surface will also depend on their chemical and physical properties. Alcohols have a substantially lower dielectric constants than H_2O ($\varepsilon = 80.4$). As a consequence, we predict that the relative thickness of the electrical double layer (EDL) should decrease when alcohols are

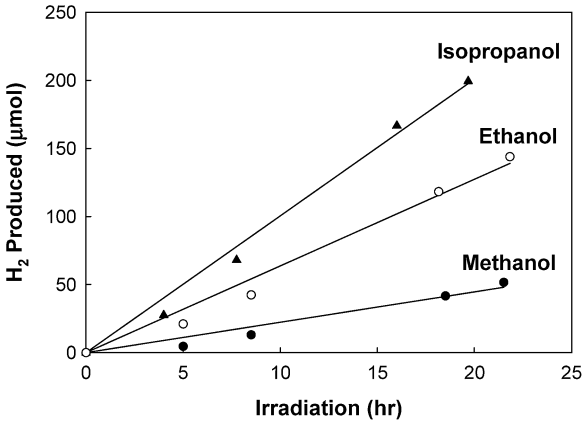

Fig. 9 Solvent effects on photocatalytic H_2 production with Ni/NiO/$KNbO_3$/CdS under visible light ($\lambda > 400$ nm).

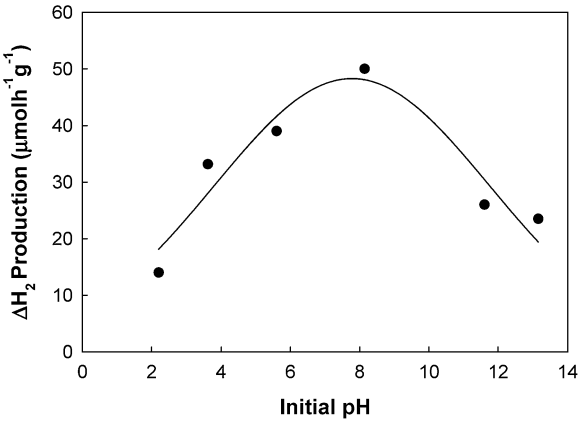

Fig. 10 pH-Dependent H_2 production from water–isopropanol mixed solution. The pH was adjusted with 0.1–1 M NaOH and HCl.

added. The EDL thickness should decrease in the order of dielectric constants, as given by the Debye equation:

$$\kappa \equiv \left(\frac{2F^2\mu}{\varepsilon\varepsilon_0 RT}\right)^{0.5} \quad (8)$$

where ε is the dielectric constant of the solvent or mixed solvent system, ε_0 is the permittivity of free space (8.854×10^{-12} C^2 J^{-1} m^{-1}), μ is the ionic strength of the background electrolyte (mol m^{-3}), R is the gas constant (8.314 J mol^{-1} K^{-1}), T is temperature in units of K, and F is the Faraday constant (96485 C mol^{-1}). Electrical double layer compression will enhance the physicochemical interaction of the electron donors with the charged CdS surface. Thus, more efficient hole trapping by the electron donors should increase H_2 production rates.

We note that SO_3^{2-} and S^{2-} are also frequently used as sacrificial donors to prevent the photocorrosion of metal sulfide semiconductors;[19,46,47,65] however, the H_2 production rate of $KNbO_3$/CdS nanocomposites with the addition of 0.01 M SO_3^{2-} and 0.1 M S^{2-} was very low relative to those with the addition of alcohols as electron donors.

Influence of pH on photocatalytic H_2 production

Without the addition of acid or base, the pH of the $KNbO_3$/CdS suspensions in ROH–H_2O is between pH 8 and 9. The pH-dependent production of H_2 from aqueous isopropanol solution under visible light is shown in Fig. 10. The highest production rates of H_2 were obtained in circumneutral pH region, while the rates of H_2 production decreased at higher and lower pH.

The relative attachment of Q-CdS on the $KNbO_3$ particles should be influenced by the $KNbO_3$ and CdS surface charges. Since the pH_{zpc} value of $KNbO_3$ was determined to be 3.2, the $KNbO_3$ surface is negatively charged at both neutral and alkaline pH (*i.e.*, pH > pH_{zpc}) and is positively charged at very acidic pH (*i.e.* pH < pH_{zpc}). In case of Q-CdS, the pH_{zpc} value varies from pH 1 to 7, according to the structure and surface characteristics of CdS, types and concentrations of background electrolytes. However, we assume that the pH_{zpc} of CdS is more likely to be high under our conditions to possibly account for the rapid attachment of CdS colloids to the larger $KNbO_3$ particles (Fig. 6(c)). Therefore, at circumneutral pH, positively charged CdS can be adsorbed onto the negatively charged $KNbO_3$ surface. At low pH, the surface charges of CdS and $KNbO_3$ would be positive, and at high pH, both particles are negatively charged so that effective contact and charge transfer from CdS to $KNbO_3$ is less likely to occur at extreme pH. Furthermore, proton ion-exchange also occurs for $KNbO_3$ samples under acidic conditions. K^+ ions in the framework of $KNbO_3$ may be ion-exchanged with H^+ ions, and the proton-exchanged form, $K_{1-x}H_xNbO_3$, may have different structure and physicochemical properties from original $KNbO_3$ materials. We prepared $K_{1-x}H_xNbO_3$ samples by stirring in 0.5 N H_2SO_4 solutions for several days followed by washing, filtration, and drying and tested the photoactivity of $K_{1-x}H_xNbO_3$/CdS nanocomposites for H_2 production. In the circumneutral pH region, $K_{1-x}H_xNbO_3$/CdS nanocomposites shows extremely low H_2 production rate ($\sim$2.8 μmol $h^{-1}g^{-1}$). Therefore, we conclude that proton-exchanged $KNbO_3$ can be formed in low pH and it may cause low photoactivity of $KNbO_3$ for H_2 production in acidic pH.

Conclusions

Efficient H_2 production was obtained with Ni/NiO/$KNbO_3$/CdS composites with visible light irradiation ($\lambda > 400$ nm). H_2 production rates were higher than for TiO_2/CdS or $K_4Nb_6O_{17}$/CdS composites. Partially reduced states of niobium (*e.g.*, Nb(IV) and Nb(III)), which are generated during Ni formation under H_2 and by photoreduction, may contribute to the enhanced reactivity of the $KNbO_3$ composites. Aliphatic alcohols (methanol, ethanol, isopropanol, *etc.*) serve as alternative electron donors and modified the near-surface environment *via* electrical double layer compression. The solution pH also influences the rate of photocatalytic H_2 production; highest H_2 production rates were obtained at circumneutral pH. In addition, the 4-component nanocomposite (Ni/NiO/$KNbO_3$/CdS) produces H_2 rapidly under natural sunlight. Our findings suggest that use of solar energy for photocatalytic water splitting with this developed photocatalyst system may give a promising source for hydrogen fuel.

Acknowledgements

We are grateful to the Hydrogen Energy Research & Development Center and 21st Century Frontier Research and Development Program of the Ministry of Science and Technology of Korea for research support.

References

1 A. Fujishima and K. Honda, *Nature*, 1972, **238**, 37.
2 K. E. Karakitsou and X. E. Verykios, *J. Catal.*, 1992, **134**, 629.
3 T. Sakata and T. Kawai, *Chem. Phys. Lett.*, 1981, **80**, 341.
4 R. Abe, T. Takata, H. Sugihara and K. Domen, *Chem. Commun.*, 2005, 3829.
5 M. A. Gondal, A. Hameed and Z. H. Yamani, *Energy Sources*, 2005, **27**, 1151.
6 D. W. Hwang, J. Kim, T. J. Park and J. S. Lee, *Catal. Lett.*, 2002, **80**, 53.
7 K. Domen, S. Naito, T. Onishi and K. Tamaru, *Chem. Phys. Lett.*, 1982, **92**, 433.
8 J. J. Zou and C. J. Liu, *Acta Phys.-Chim. Sin.*, 2006, **22**, 926.
9 A. J. Hoffman, H. Yee, G. Mills and M. R. Hoffmann, *J. Phys. Chem.*, 1992, **96**, 5540.
10 K. Maeda, T. Takata, M. Hara, N. Saito, Y. Inoue, H. Kobayashi and K. Domen, *J. Am. Chem. Soc.*, 2005, **127**, 8286.
11 A. Steinfeld, *Int. J. Hydrogen Energy*, 2002, **27**, 611.
12 M. Ashokkumar, *Int. J. Hydrogen Energy*, 1998, **23**, 427.
13 G. C. De, A. M. Roy and S. S. Bhattacharya, *Int. J. Hydrogen Energy*, 1996, **21**, 19.
14 D. N. Furlong, F. Grieser, D. Hayes, R. Hayes, W. Sasse and D. Wells, *J. Phys. Chem.*, 1986, **90**, 2388.
15 G. Q. Guan, T. Kida, K. Kusakabe, K. Kimura, X. M. Fang, T. L. Ma, E. Abe and A. Yoshida, *Chem. Phys. Lett.*, 2004, **385**, 319.
16 N. Kakuta, K. H. Park, M. F. Finlayson, A. Ueno, A. J. Bard, A. Campion, M. A. Fox, S. E. Webber and J. M. White, *J. Phys. Chem.*, 1985, **89**, 732.
17 N. Z. Muradov, M. I. Rustamov, A. D. Guseinova and Y. V. Bazhutin, *React. Kinet. Catal. Lett.*, 1987, **33**, 279.
18 J. Kobayashi, K. Kitaguchi, H. Tanaka, H. Tsuiki and A. Ueno, *J. Chem. Soc., Faraday Trans. 1*, 1987, **83**, 1395.
19 A. Koca and M. Sahin, *Int. J. Hydrogen Energy*, 2002, **27**, 363.
20 K. Domen, A. Kudo, M. Shibata, A. Tanaka, K. Maruya and T. Onishi, *J. Chem. Soc., Chem. Commun.*, 1986, 1706.
21 A. Furube, T. Shiozawa, A. Ishikawa, A. Wada, K. Domen and C. Hirose, *J. Phys. Chem. B*, 2002, **106**, 3065.
22 S. Ikeda, A. Tanaka, K. Shinohara, M. Hara, J. N. Kondo, K. I. Maruya and K. Domen, *Microporous Mater.*, 1997, **9**, 253.
23 K. Sayama, A. Tanaka, K. Domen, K. Maruya and T. Onishi, *Catal. Lett.*, 1990, **4**, 217.
24 K. Sayama, A. Tanaka, K. Domen, K. Maruya and T. Onishi, *J. Phys. Chem.*, 1991, **95**, 1345.
25 S. Ikeda, M. Fubuki, Y. K. Takahara and M. Matsumura, *Appl. Catal., A*, 2006, **300**, 186.
26 H. Kato and A. Kudo, *J. Phys. Chem. B*, 2001, **105**, 4285.
27 M. Machida, T. Mitsuyama, K. Ikeue, S. Matsushima and M. Arai, *J. Phys. Chem. B*, 2005, **109**, 7801.
28 M. Machida, J. Yabunaka and T. Kijima, *Chem. Mater.*, 2000, **12**, 812.
29 S. Kim, S. J. Hwang and W. Y. Choi, *J. Phys. Chem. B*, 2005, **109**, 24260.
30 D. F. Wang, J. H. Ye, T. Kako and T. Kimura, *J. Phys. Chem. B*, 2006, **110**, 15824.
31 D. E. Gu, B. C. Yang and Y. D. Hu, *Catal. Lett.*, 2007, **118**, 254.
32 J. L. Gole, J. D. Stout, C. Burda, Y. B. Lou and X. B. Chen, *J. Phys. Chem. B*, 2004, **108**, 1230.
33 H. Kisch, S. Sakthivel, M. Janczarek and D. Mitoraj, *J. Phys. Chem. C*, 2007, **111**, 11445.
34 K. R. Reyes-Gil, E. A. Reyes-Garcia and D. Raftery, *J. Phys. Chem. C*, 2007, **111**, 14579.
35 S. Yin, M. Komatsu, Q. W. Zhang, F. Saito and T. Sato, *J. Mater. Sci.*, 2007, **42**, 2399.
36 Y. Murakami, B. Kasahara and Y. Nosaka, *Chem. Lett.*, 2007, **36**, 330.
37 J. C. Yu, W. K. Ho, J. G. Yu, H. Yip, P. K. Wong and J. C. Zhao, *Environ. Sci. Technol.*, 2005, **39**, 1175.
38 H. Liu, A. Imanishi and Y. Nakato, *J. Phys. Chem. C*, 2007, **111**, 8603.
39 W. U. Zhang, Y. Zhong, J. Fan, S. Q. Sun, N. Tang, M. Y. Tan and L. M. Wu, *Sci. China Ser. B*, 2003, **46**, 196.
40 C. A. Linkous, N. Z. Muradov and S. N. Ramser, *Int. J. Hydrogen Energy*, 1995, **20**, 701.
41 A. M. Roy and G. C. De, *J. Photochem. Photobiol., A*, 2003, **157**, 87.
42 D. W. Bahnemann, C. Kormann and M. R. Hoffmann, *J. Phys. Chem.*, 1987, **91**, 3789.
43 A. J. Hoffman, G. Mills, H. Yee and M. R. Hoffmann, *J. Phys. Chem.*, 1992, **96**, 5546.
44 Y. Bessekhouad, N. Chaoui, M. Trzpit, N. Ghazzal, D. Robert and J. V. Weber, *J. Photochem. Photobiol., A*, 2006, **183**, 218.
45 F. Chen, Y. P. Zhu, H. L. Ma, Z. L. Bo and J. L. Zhang, *Acta Phys.-Chim. Sin.*, 2004, **20**, 1292.
46 J. S. Jang, W. Li, S. H. Oh and J. S. Lee, *Chem. Phys. Lett.*, 2006, **425**, 278.
47 S. V. Tambwekar, D. Venugopal and M. Subrahmanyam, *Int. J. Hydrogen Energy*, 1999, **24**, 957.
48 M. Innocenti, S. Cattarin, F. Loglio, T. Cecconi, G. Seravalli and M. L. Foresti, *Electrochim. Acta*, 2004, **49**, 1327.
49 A. Ueno, N. Kakuta, K. H. Park, M. F. Finlayson, A. J. Bard, A. Campion, M. A. Fox, S. E. Webber and J. M. White, *J. Phys. Chem.*, 1985, **89**, 3828.
50 J. Yoshimura, A. Tanaka, J. N. Kondo and K. Domen, *Bull. Chem. Soc. Jpn.*, 1995, **68**, 2439.
51 W. F. Shangguan and A. Yoshida, *Sol. Energy Mater. Sol. Cells*, 2001, **69**, 189.
52 W. F. Shangguan and A. Yoshida, *J. Phys. Chem. B*, 2002, **106**, 12227.
53 K. Domen, A. Kudo, T. Onishi, N. Kosugi and H. Kuroda, *J. Phys. Chem.*, 1986, **90**, 292.
54 A. Kudo, A. Tanaka, K. Domen, K. Maruya, K. Aika and T. Onishi, *J. Catal.*, 1988, **111**, 67.
55 M. Ewart, I. Biaggio, M. Zgonik and P. Gunter, *Phys. Rev. B*, 1994, **49**, 5263.
56 J. M. Kesselman, O. Weres, N. S. Lewis and M. R. Hoffmann, *J. Phys. Chem. B*, 1997, **101**, 2637.
57 A. Yariv, S. S. Orlov and G. A. Rakuljic, *J. Opt. Soc. Am., B*, 1996, **13**, 2513.
58 G. Montemezzani and P. Gunter, *J. Opt. Soc. Am. B*, 1990, **7**, 2323.
59 S. W. Park and C. P. Huang, *J. Colloid Interface Sci.*, 1987, **117**, 431.
60 J. C. Liu and C. P. Huang, *Langmuir*, 1992, **8**, 1851.
61 J. D. G. Duran, M. C. Guindo, A. V. Delgado and F. GonzalezCaballero, *J. Colloid Interface Sci.*, 1997, **193**, 223.
62 M. C. Guindo, L. Zurita, J. D. G. Duran and A. V. Delgado, *Mater. Chem. Phys.*, 1996, **44**, 51.
63 Y. F. Nicolau and J. C. Menard, *J. Colloid Interface Sci.*, 1992, **148**, 551.
64 K. Domen, J. N. Kondo, M. Hara and T. Takata, *Bull. Chem. Soc. Jpn.*, 2000, **73**, 1307.
65 T. Uchihara, M. Matsumura and H. Tsubomura, *J. Phys. Chem.*, 1989, **93**, 3207.

